A review of radiative detachment studies in tokamak advanced magnetic divertor configurations

IOP Publishing Plasma Physics and Controlled Fusion
Plasma Phys. Control. Fusion **59** (2017) 064005 (12pp) https://doi.org/10.1088/1361-6587/aa6959

A review of radiative detachment studies in tokamak advanced magnetic divertor configurations

V A Soukhanovskii

Lawrence Livermore National Laboratory, 7000 East Ave, Livermore, CA 94550, United States of America

E-mail: vlad@llnl.gov

Received 21 December 2016, revised 16 March 2017
Accepted for publication 27 March 2017
Published 28 April 2017

Abstract

The present vision for a plasma–material interface in the tokamak is an axisymmetric poloidal magnetic X-point divertor. Four tasks are accomplished by the standard poloidal X-point divertor: plasma power exhaust; particle control (D/T and He pumping); reduction of impurity production (source); and impurity screening by the divertor scrape-off layer. A low-temperature, low heat flux divertor operating regime called radiative detachment is viewed as the main option that addresses these tasks for present and future tokamaks. Advanced magnetic divertor configuration has the capability to modify divertor parallel and cross-field transport, radiative and dissipative losses, and detachment front stability. Advanced magnetic divertor configurations are divided into four categories based on their salient qualitative features: (1) multiple standard X-point divertors; (2) divertors with higher order nulls; (3) divertors with multiple X-points; and (4) long poloidal leg divertors (and also with multiple X-points). This paper reviews experiments and modeling in the area of radiative detachment in the advanced magnetic divertor configurations.

Keywords: tokamak, divertor, detachment, snowflake divertor, advanced divertor

(Some figures may appear in colour only in the online journal)

1. Introduction

Based on nearly five decades of magnetically confined nuclear fusion plasma physics research, an axisymmetric poloidal magnetic X-point divertor has become the present vision for a tokamak plasma–material interface. The divertor concept is credited in the literature [1, 2] to Spitzer who proposed it for a stellarator [3]. The poloidal magnetic X-point divertor was later adopted for the toroidally symmetric tokamak [4–6]. In the tokamak, a magnetic X-point is created between two toroidal currents—a plasma current and a special magnetic coil. A formed magnetic separatrix divides the plasma into a closed field line region (confined plasma) and an open field line scrape-off layer (SOL) region. The SOL is directed (diverted) into a special divertor chamber and terminated on a target plate. The poloidal divertor enables energy and particles lost from the confined core plasma due to radial transport and magneto-hydrodynamic (MHD) instabilities (e.g., edge localized modes (ELMs)) to flow to the divertor chamber that acts as a separate plasma–material interface. Four tasks are accomplished by the standard poloidal X-point divertor (e.g., [2]): (1) plasma power exhaust; (2) particle control (D/T and He pumping); (3) impurity production (source) reduction; (4) impurity screening by the divertor SOL.

The divertor SOL parallel heat transport is dominated by electron conduction and convection and strongly depends on plasma collisionality [2, 7, 8]. At higher plasma collisionality, a low-temperature highly radiative divertor regime sets in: the plasma flowing to divertor plates looses energy through radiation and dissipative processes, and momentum through charge exchange, inelastic collisions and recombination. This leads to plasma neutralization and detachment from the target plate, and as a result, significantly reduced heat load and material erosion. The radiative regime is commonly called radiative plasma detachment. It is characterized by a parallel SOL electron (plasma) pressure drop, high neutral divertor pressure (density),

Table 1. A comparison of power and divertor conditions in present day tokamaks, ITER and DEMO devices [9–11].

	Present day tokamaks	ITER	DEMO
P_{heat}/R (MW m^{-1})	⩽27	⩽20	80–100
q_{peak} (MW m^{-2})	⩽5–15	⩽50	100–300 Unmitigated
$q_{\|\|}$ (MW m^{-2})	100–2000	5000	30000 Unmitigated

low plasma electron temperature ($T_e \leqslant$ 1–2 eV), high electron density at the plate, and high impurity radiation. It is viewed as the main solution to tokamak power and particle exhaust within operating limits of plasma-facing component cooling technology and target materials. The proposed ITER divertor is based on standard X-point divertor geometry designs tested in large tokamak experiments: vertical targets with partial radiative detachment of the strike points are used. The term partial here refers to the plasma detachment from the plate only in the radial region adjacent to the separatrix, as the full detachment, while highly desirable for impurity erosion reduction, is likely to lead to confinement degradation via an X-point radiative instability. However, in high-power tokamak devices beyond ITER such as the proposed fusion nuclear science facilities or the DEMO reactor, divertor radiation may be insufficient for mitigating power loads. Compared in table 1 are three metrics, the P_{heat}/R, the steady-state peak divertor heat flux q_{peak}, and steady-state upstream (before divertor entrance) parallel heat flux $q_{\|}$ in present-day devices, ITER, and some DEMO concepts [9–11]. The comparison demonstrates significant gaps between the present state of physics and technology and DEMO-class device requirements, which typically must rely on highly radiative divertor solutions, with radiated power fractions up to 80%–90% of total input power.

Magnetic divertor configuration development aimed at optimizing particle and power exhaust has been an active area of fusion research since the 1970s. Many magnetic divertor configuration concepts (arguably 'advanced' w.r.t. the standard X-point divertor) may be able to modify parallel and perpendicular transport, dissipative loss channels, and increase plasma-wetted area. Power and particle exhaust can also be improved via optimization of the standard X-point divertor using 'non-magnetic' means, i.e., divertor target geometry including divertor closure [12–14], target plate electric biasing, liquid metal targets, liquid metal curtains, moving divertor plates, or moving pebbles (e.g., [15]). However, these concepts are outside of the present review. In this paper, only 'advanced' magnetic divertor configurations are reviewed with emphasis on their potential improvement of the radiative (detached) power exhaust, since the future reactor-class devices are likely to benefit from both approaches.

The paper is organized as follows. In section 2 we discuss how the radiative detachment regime may be improved via magnetic divertor parameters. Section 3 provides a brief historical perspective on advanced magnetic divertor configuration development. Advanced magnetic divertor configurations are divided in four categories based on the following salient qualitative features: (1) multiple standard X-point divertors; (2) higher order null divertors; (3) divertors with multiple X-points; (4) long-legged divertors (and also with multiple X-points). Section 4 reports on the status of experimental and modeling results obtained to date in some of these configurations. A brief discussion in section 5 concludes the review.

2. Advanced divertor configuration effects on radiative detachment

Radiative divertor detachment is a complex multi-physics phenomena. A number of reviews (e.g., [7, 8, 19, 20] and those included in this journal issue) explain the physics and phenomenology of divertor detachment in tokamaks, and in the following, we refrain from repeating it. There are areas of divertor detachment physics that are not yet fully understood or included in the present physics models, such as, e.g., divertor turbulence and radial transport, transition to detachment, detachment front stability, radiation distribution, kinetic effects, and impact of cross-field drifts. However, the basic physics processes appears to be understood well enough to predict the shortcomings of the radiative divertor in the standard X-point configuration at very high tokamak power, thus providing motivation for advanced magnetic configuration research.

For illustration, consider peak divertor heat flux q_{peak} at the outer strike point of the lower single null X-point configuration. It can be approximated as a ratio of the divertor outer leg power P_{div} and the outer divertor plasma-wetted area A_{wet} [21, 22]:

$$q_{peak} \sim \frac{P_{div}}{A_{wet}} = \frac{P_{heat}(1-f_{rad})f_{out/tot}f_{down/tot}(1-f_{pfr})\sin\alpha}{N_{div}2\pi R_{SP}f_{exp}\lambda_{q_{\|}}}, \quad (1)$$

where P_{heat} is the input heating power, f_{rad}, $f_{down/tot}$, $f_{out/tot}$, and f_{pfr} are fractions of power going to radiation, lower divertor, outer divertor, and private flux regions, respectively; α is the divertor plate poloidal tilt angle (a deviation from an orthogonal plate); and R_{SP} is the strike point radius. The poloidal magnetic flux expansion is

$$f_{exp} = B_p^{SP}R_{mp}/(B_p^{mp}R_{SP}), \quad (2)$$

where B_p and R are the poloidal magnetic field and major radii of the flux tube at the strike point (SP) and mid-plane (MP) locations. This simplified formula shows how advanced divertor configurations may help with divertor heat flux mitigation: (1) increase plasma wetted area A_{wet}, e.g., via poloidal magnetic flux expansion and increased SOL power width λ_q in the divertor (via increased divertor radial transport and/or increased connection length). (2) Increase the number of divertors (legs, strike points); (3) increase of radiated

power and momentum losses via increased divertor volume and connection length; (4) increase of divertor area at larger R_{SP}. The connection length is a magnetic field line length from the X-point (or from midplane) to the strike point taken close to separatrix:

$$l_{\parallel} = \int_{SP}^{X\,(MP)} \frac{\sqrt{B_t^2 + B_p^2}}{B_p} \mathrm{d}l. \quad (3)$$

Furthermore, if one is interested in optimizing detachment, zero-dimensional physics arguments based on a simplified picture of conductive power flow balanced by volumetric losses (e.g., [2, 23]), yield a simple detachment criterion:

$$\frac{14}{3} c_Z L_Z n_u^2 l_{\parallel} > q_u, \quad (4)$$

where c_Z is impurity fraction, L_Z is plasma radiation efficiency, n_u is upstream density, and q_u is the parallel upstream heat flux. This zero-order criterion highlights experimental routes to detachment in the standard divertor [2], and also highlights the areas where advanced magnetic divertor configurations can facilitate or enhance detachment. These are essentially the areas that present research is attempting to clarify in order to assess the potential of the advanced magnetic configurations: increasing non-coronal radiation efficiency L_Z; better entraining impurities enabling higher divertor c_Z; reducing q_u by sharing SOL power among several divertors or strike points $P_{SOL} \sim q_u$; increasing connection length $l_{\parallel}$ by lowering B_p, elongating the divertor leg, that would lead to lowering divertor T_e; and increasing n_u (or $n_{div} \sim n_u^3$).

In addition to the areas illustrated above, other directions arise from either two-dimensional analyses, or from integrated solution arguments (e.g., [24]). The density n_u, for example, must be kept lower due to tokamak performance requirements (i.e., current drive, NBI efficiency, density limit), hence the 'detachment operating window' is a critical parameter: one is interested in having a detached divertor at a minimum possible upstream density. Another consideration is keeping the 'detachment front' (which refers to the plasma recombination region) or the radiation front (which refers to the impurity radiation region) away from the main separatrix, to prevent confinement degradation. One is also interested in the SOL detachment over the entire extent of the SOL to reduce material erosion. Finally, divertor physics is inherently two or even three-dimensional, and must include complex details of parallel and cross field transport and turbulence, neutral density (pressure) distribution that are all critically important. In this paper, we review how the radiative divertor concept may be improved by advanced magnetic configurations over the standard divertor configuration along the lines discussed above.

3. Concepts overview via historical perspective

Novel magnetic divertor configuration development and divertor optimization has always been an active area in fusion plasma research. The concept development was driven by many factors: priorities varied with physics understanding and fusion program considerations over the years. In the early days of tokamak research, e.g., before the 1980s, emphasis was placed on impurity and recycling control, since the magnetic divertor was viewed as a better configuration (compare to the limiter) for impurity screening and reduction [25, 26]. In many early concepts, the divertor was called a burial chamber and the divertor target plates were referred to as neutralizer plates, to emphasized the impurity control and recycling aspects. However, in later years, tokamak reactor designs became more conceptually mature: nuclear science and technology driven considerations, such as, e.g., shielding of components from intense neutron irradiation, cooling technology including cooling agents, poloidal magnetic coil design and placement, highlighted obvious shortcomings of many early concepts [27].

First poloidal X-point divertors were implemented on the JFT2/DIVA and T12 tokamaks in the 1970s [28–31]. From the early 1980s, while divertor experiments still focused on recycling and impurity control [32–37], both the power and particle handling topics came into focus of conceptual development (e.g., [38]. A cold gas target high-density divertor concept (that later evolved into the radiatively detached divertor) was known from the 1970s [39]. It was first implemented and developed in the 1980s [40–46]. Significant research progress was made in the 1990s: the radiative detachment was studied in large tokamaks with high input power, density control via cryopumping, and large divertor radiated power fractions relevant to reactor-like conditions [7, 8, 19, 23]. In parallel, attention turned to advanced magnetic configurations and their potential for attractive solutions based on combined magnetic and radiative properties [47]. In the past decade and a half (2000-present time), fusion research re-focused its efforts on the plasma–material interface, and many old concepts were re-discovered. We now briefly review advanced magnetic divertor configurations in order to provide background for discussion of recent experimental and modeling research efforts.

Multiple standard divertors. Configurations with multiple standard X-point divertors are advanced in a sense that the SOL power P_{SOL} is shared among N divertors [2]. At reduced power, each standard divertor may have a reduced detachment threshold expressed in terms of n_e and c_Z. Additional divertors may also be placed at a larger R, thereby affording a larger A_{wet} and a longer $l_{\parallel}$. Present day tokamaks are built with up-down symmetric sets of divertor coils that offer a capability of two standard X-point divertors commonly referred to as double null (DN) configurations. Such DN configurations have been envisioned for many tokamak concepts [48–51] and realized in a number of tokamaks (e.g., [16, 52, 53]) (see figure 1). The DN divertor provides heat and particle sharing between divertors [54], a possibility of separating power and particle control [55, 56], and unique quiescent properties of the inner isolated SOL [57]. Triple and quadrupole divertors has also been implemented and studied (figure 1). Theoretical analysis of a triple X-point divertor concept suggested that it may facilitate the D-shaped high-

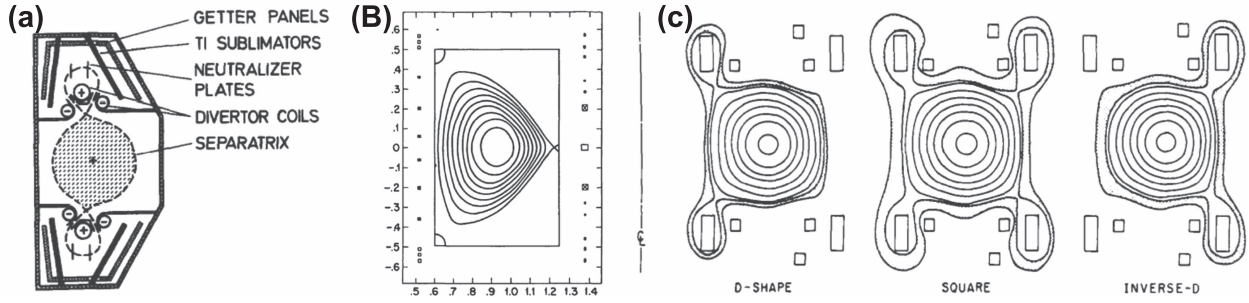

Figure 1. Standard divertor configurations with (a) two divertors (DN) implemented in ASDEX (Reprinted from [16] Copyright 1980, with permission from Elsevier.), (b) three divertors (Reproduced courtesy of IAEA. Figure from [17]. Copyright 1990 IAEA.), and (c) two and four divertors implemented in PDX (Reprinted from [18] Copyright 1980, with permission from Elsevier.).

triangularity plasmas with increased local magnetic shear leading to enhanced kink stability and reduced drift-wave turbulent transport [17]. The triple X-point divertor configuration has been produced in the TCV tokamak [58]. Configurations with DN and four null (eight leg) divertors have been implemented in the poloidal divertor experiment (PDX) tokamak.

Second- and third-order null divertors. Recent analyses of divertor magnetic field structure led to new high-order poloidal field null configurations: the snowflake [59] and the cloverleaf [60] divertors shown in figure 2. The higher order nulls are obtained by superimposing standard (first-order) poloidal field nulls (X-points). The snowflake configuration has a second order null where the magnetic field scales as r^2 with the distance r from the null, whereas the cloverleaf's third order null region yields a $B_p \sim r^3$ scaling. The naming convention is derived based on the separatrix appearances of a snowflake and a clover leaf, respectively (figure 2): the snowflake has four divertor separatrix branches (legs, strike points) and the cloverleaf has six. In both configurations, a larger area of a weak poloidal field is formed (compare to standard divertor). The exact snowflake and cloverleaf configurations are topologically unstable due to fluctuations of divertor coil and plasma time-varying currents and magnetic fluxes, so in practice there is always finite but small distance

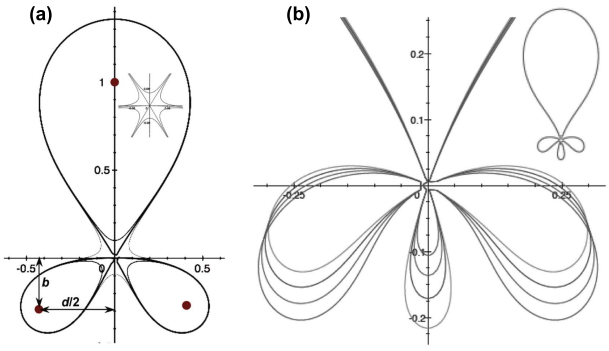

Figure 2. (a) The snowflake divertor configuration (Reprinted from [59], with permission of AIP Publishing.) and (b) the cloverleaf divertor configuration (Reprinted from [60], with permission of AIP Publishing.).

between the two or three nulls, respectively. A larger region of low B_p may significantly modify divertor heat and particle transport and deposition. From the divertor geometry arguments, the snowflake divertor has a potential to increase divertor radiated power and ion momentum losses via longer connection length and greater flux tube volume, and larger divertor physical volume due to expanded flux tubes. Transport and drift effects, e.g., increased radial transport and modification in the parallel impurity transport, as well as predicted enhanced ion losses [61], can play a role, especially in view of sharing the power between additional divertor legs [62]. Since snowflake divertor configurations have additional strike points (divertor legs), one of the main questions is the sharing of heat and particle fluxes between them due to convective plasma mixing, as predicted by theory [63], and detachment of individual legs. The snowflake divertor has been implemented in several tokamaks: TCV, NSTX, DIII-D, and EAST. The experimental results and the snowflake theory and modeling developments have been reviewed recently [62]. The cloverleaf configuration has been demonstrated in the TCV tokamak [58]. Radiative snowflake divertor experiments and modeling are reviewed section 4.

High-flux expansion divertors with multiple X-points. A number of advanced divertor configurations feature a large poloidal flux expansion $f_{\rm exp}$ at the strike point. The flux tubes are expanded by nearby additional poloidal field null(s)) created by either axisymmetric (e.g., [52, 64–66]) or additional non-axisymmetric dipole divertor coils [67–71]. The configuration, in its extreme, resembles the cusp magnetic field obtained with dipole coils [72] as proposed in the cusp divertor configuration [69] shown in figure 3(a). An identical configuration was later called an X-divertor [70] (figure 3(b)). While the increased poloidal magnetic flux expansion $f_{\rm exp}$ can significantly reduce peak divertor heat flux via increased plasma wetted area, it cannot by itself solve the integrated power and particle exhaust problem. The flux expansion is limited by the angle between the total magnetic field line and the divertor plate, since the angle must conform to engineering requirements (typically $\alpha \geqslant 1^\circ$). Additional advantages of these configurations for detachment include the increased connection length and increased divertor leg volume that can accommodate higher neutral and impurity inventory, and lead to increased radiative losses, lowering plasma T_e, and reduced penetration of neutrals. A special feature

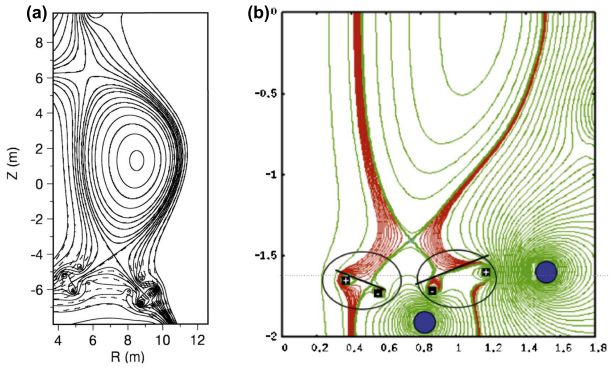

Figure 3. High-flux expansion divertors with multiple X-points obtained with dipole coils: (a) the cusp divertor (Reproduced with permission of [69]) and (b) the X-divertor (Reprinted from [73], with the permissions of AIP Publishing.)

of the cusp/X-divertor—a magnetic field line flaring (a converging–diverging field line geometry) due to the second X-point near the divertor plate—was analyzed with respect to detachment front stabilization. References [73, 74] describe a qualitative picture of how the magnetic flux tube flaring throughout a high neutral density region could stabilize the ionization-recombination front and prevent it from moving upstream, thereby creating a possibility of a fully detached divertor with a stabilized detachment front. Reference [73] included a measure of local field line flaring called a divertor index, and used it to argue that the physics of experimental snowflake divertor configurations with closely positioned divertor target plates could be attributed to X-divertor effects. In [75], both of these conjectures have been argued to be erroneous on the accounts of oversimplification of divertor physics and focusing on certain magnetic features while ignoring others. Details of this argument are outside of this review. The divertor index is not used in the cusp/X divertor studies reviewed in section 4. The high flux expansion divertor configurations have been studied in several experiments as well as using two-dimensional models and are also reviewed in section 4.

Long-legged divertors (also with additional X-points). Long-legged divertors were considered in many early tokamak reactor concepts (before 1980s) as they were viewed as offering a plasma–material interface removed from the main plasmas, as in, e.g., the Princeton reactor [77–79], the UWMAK series devices [49, 80–84], and others [85], including radiative long-legged divertors [47]). Here we generally refer to the poloidal divertor leg length. A number of long-legged divertor concepts also included multiple nulls due to many divertor coils that were used to guide a long plasma channel (divertor leg) away from the main plasma. The divertor targets were placed inside or outside the toroidal field coil contour [85, 86], and even inner long legs extending to a large major radius were proposed [84, 85, 87]. The long-legged multiple null divertors were often combined with cryo-panels for particle control, liquid metal targets, and featured large magnetic flux expansions at the strike points. Some examples of these configurations are shown in figure 4. The main disadvantage of these concepts is increased technical and plasma control complexities due to a large number

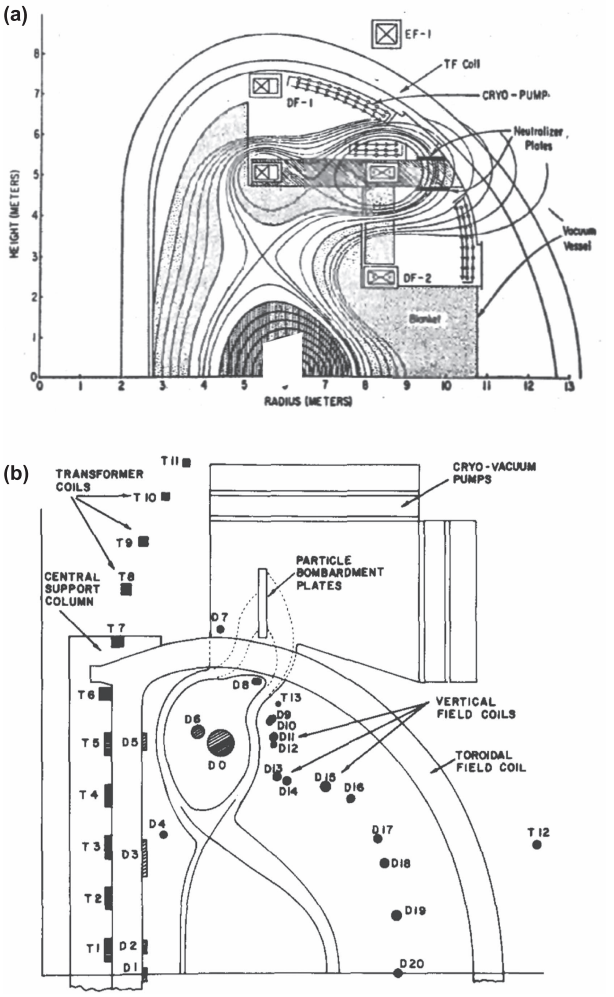

Figure 4. Reactor concepts with long poloidal leg high-flux expansion divertors: (a) experimental tokamak reactor (Reprinted with permission [85] © 1975 IEEE.) and (b) UWMAK-II (Reprinted from [49] Copyright 1976, with permission from Elsevier.).

of coils, and an excessive utilization of physical space inside the toroidal field coil, potentially resulting in larger device size and prohibitive costs. Despite the engineering complexities, new long-legged multiple-null divertor concepts have been recently proposed: (1) the Super-X divertor and (2) the X-point target divertor. These configurations are shown in figure 5. The Super-X concept combines a long poloidal leg with the divertor target at the largest possible radius. It may also include a high poloidal flux expansion at the target as in the cusp/X-divertor [88, 89]. The X-point target divertor features a long poloidal divertor leg with an additional null in the plasma at the target plate [57]. Long-legged divertors (with and without additional X-points) offer a number of potential benefits for detachment physics. One advantage of the configurations with long poloidal legs is the possibility of increased radial heat transport over the increased connection length that may lead to a reduced target temperature. A long poloidal leg may also offer increased radiating volume and a possibility of tight baffling, all potentially leading to reduced $q_{||}$ and T_e at the target, higher neutral

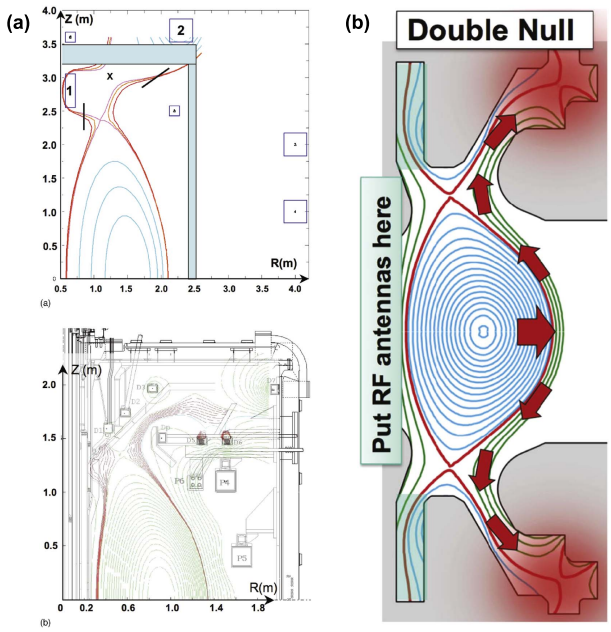

Figure 5. (a) Super-X divertor configurations designed for a tokamak compact fusion neutron source, and an initial design of MAST Upgrade (Reprinted from [88], with permission of AIP Publishing.); (b) X-point target configuration for advanced divertor and radio-frequency tokamak experiment concept (Reproduced courtesy of IAEA. Figure from [57]. Copyright 2015 IAEA.).

density, and the detachment radiation front stabilization away from the main X-point. If the long poloidal leg divertor strike point is moved to a larger major radius, this could lead to increased target area ($\sim R^2$) and reduced $q_{||}$ due to toroidal flux expansion (B_X/B_R). The introduction of additional X-points in the target area may bring additional benefits for detachment. The Super-X divertor with an additional X-point under the target may stabilize detachment front far away from the main plasma by strong flux tube flaring, and increase radiated power and momentum loss via increased divertor leg volume. The X-point target divertor may stabilize the detachment front by an additional X-point that acts as a virtual target in a remote divertor chamber where most of radiation and momentum loss occur. The Super-X divertor configuration has been created in the TCV tokamak (albeit without additional poloidal flux expansion in the divertor leg) [90], and is being implemented in a special divertor geometry of MAST Upgrade tokamak [91, 92]. The X-point target configuration has been implemented in the TCV tokamak [90]. Long divertor leg effects have been studied in several tokamak experiments and numerical models of various degrees of complexity. These divertor concepts are reviewed in section 4.

4. Studies of radiative plasma detachment in advanced magnetic divertor configurations

The present status of experimental and modeling studies of detachment in advanced magnetic configurations is reviewed in this section. We start with results from first divertor experiments conducted in the 1980s in the Axially Symmetric

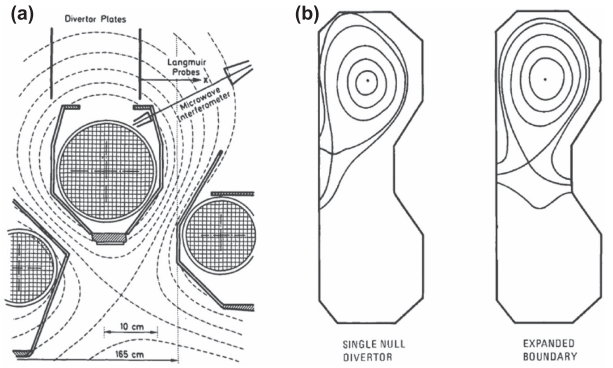

Figure 6. (a) ASDEX DN divertor configuration with expanded (flaring) flux tubes (Reproduced courtesy of IAEA. Figure from [41]. Copyright 1983 IAEA.) and (b) single null high-flux expansion and expanded boundary divertor configurations realized in Doublet III (Reprinted from [93], with the permission of AIP Publishing.).

Divertor EXperiment (ASDEX), Doublet III, PDX and JT-60 tokamaks. Shown in figures 1 and 6 are representative divertor configurations [38] from these experiments. As can be seen, some of the early divertor configurations were prototypical of the recently proposed advanced magnetic configurations. The ASDEX and PDX implemented DN and four-null divertor configurations; flux surfaces in the ASDEX divertor flared toward divertor plates increasing poloidal magnetic flux expansion, hence the resemblance to the cusp/X-divertor. In Doublet III, single-null divertor configuration had high flux expansion and long legs, whereas the expanded boundary configuration in addition had a secondary poloidal field null in the private flux region, hence its resemblance to quasi-snowflake configurations. Later in this section, we focus on several concepts that attracted much interest recently: the DN configuration, the long legged divertor (the long poloidal leg, the Super-X, the X-point target), divertors with large flux expansion and/or flux tube flaring (the cusp/X-divertor), and the snowflake divertor configurations.

First experiments conducted in magnetic divertor tokamaks ASDEX, Doublet III, PDX and JT-60 focused on general divertor studies [18, 94–97], including impurity screening [36, 98–100], helium ash exhaust [101–103], power balance and divertor heat deposition in ohmic and NBI-heated discharges [46, 104], and access to improved confinement regimes (H-mode) [105–107]. Low-recycling (sheath-limited), high-recycling and remote radiative cooling divertor regimes were also studied [108].

ASDEX operated in a DN configuration, each divertor had three internal divertor coils, tight baffling and titanium target plates [52, 109]. Gas puffing and variable divertor throat closure were used, among other actuators, to manipulate parallel temperature gradient and reach the low $T_e \sim 7$ eV, high n_e divertor regime in H-mode plasmas with $P_{\mathrm{NBI}} \simeq 2.5$ MW power. Divertor regimes (sheath-limited, high-recycling) and their dependence on density (collisionality) were studied [41].

The PDX experiments were conducted in single, DN, and four-null configurations. Each divertor was formed using

dedicated 3–4 divertor coils inside a vacuum vessel. Titanium-coated divertor plates were used. Low T_e, high n_e divertor regimes in NBI-heated discharges with up to 4.5 MW and significant divertor radiation were studied [110]. In this regime, heat flux profiles were found to broaden with increasing density, accompanied by peak heat flux reduction. It was suggested that plasma radiation and charge exchange were responsible for the divertor power losses [111]. Double- and four-null configurations were routinely produced, however, the most notable PDX contributions to edge fusion physics, such as, e.g., the discoveries of the H-mode and the ELMs, were obtained in the DN configuration [105].

The Doublet III tokamak used 24 poloidally distributed magnetic shaping coils outside of the vacuum vessel (see internal divertor coils in ASDEX, PDX and JT-60). D-shaped elongated plasmas ($\kappa \leqslant 1.6$) with $I_p = 1$–2 MA were produced [112]. Inconel limiters mounted on inner and outer sides of the elongated vacuum vessel were used as target plates in an open geometry single null and expanded boundary divertor (figure 6). The outer strike point could be placed either on the inner side or on the outer side, resulting in a high-flux expansion outer divertor leg at different R. The 'remote radiation cooling' regime in the standard and the expanded boundary configurations was quantitatively studied in ohmic and NBI-heated (up to 2 MW) plasmas, where reduced heat flux due to radiation with increasing density and main plasma impurity reduction were found [42, 46, 113, 114]. Similar findings came from the H-mode experiments with up to 7.5 MW NBI-heating and with argon injection [115]. Detailed measurements of divertor parameters showed the parallel electron pressure drop and divertor $T_e \leqslant 10$ eV [116, 117].

These divertor experiments were able to achieve highly radiative conditions, however, generally did not reach very low temperatures $T_e \leqslant 1$–2 eV that are presently understood necessary for transition to plasma detachment. From the three mentioned experiments, Double III expanded boundary were probably the most relevant to the subject of detachment in advanced magnetic configurations as it reached the lowest electron temperatures, possibly due to its geometry and the associated additional momentum and power losses. However, neither of the experiments specifically focused on the advanced magnetic configuration effects. In parallel, divertor model development and one- and two-dimensional fluid modeling of these experiments enabled understanding of the divertor low-recycling, high-recycling and highly radiative regimes, including numerical demonstration of properties like parallel electron pressure drop, momentum loss, recycling and radiative cooling [118–120].

Significant progress in detachment physics understanding was achieved from the late 1980s to the 2000s in the standard tokamak divertor configuration in Alcator C-Mod, ASDEX-U, DIII-D, JET, JT-60 and JT-60U and simultaneously in theory and modeling [7, 8, 19]. The results led to a physics-based design of the vertical-plate ITER divertor with a dome [121–123]. A number of important physics processes were clarified, e.g. the parallel T_e gradient, electron pressure loss, radiation front formation and stability, multifaceted asymmetric radiation instabilities, and electron–ion recombination. In the course of these studies in the 1990s, some geometric features associated with advanced magnetic geometries, had come into focus: the poloidal magnetic flux expansion and magnetic field line connection length, and their role in detachment physics [12, 19, 124, 125].

Radiative DN divertors. Radiative divertor studies in the DN configuration have been a focus of DIII-D experiments using cryopumping for particle exhaust, induced SOL flow for seeded impurity (argon) entrainment ('puff-and-pump' techniques), and neon seeding [54–56, 126]. These experiments not only focused on divertor characteristics, but also combined it with high core performance plasmas with high $\beta_N \simeq 3$ and high confinement factors $H_{98(y,2)} \simeq 1.35$, and high input power. About 60% of the input power $P_{\rm in} = 10$ MW was exhausted through divertor radiation, resulting in a significant reduction of target heat fluxes. These experiments clearly demonstrated the radiative DN potential as an integrated plasma–material interface.

High flux expansion (cusp, X-, tripod) divertor. Several experiments studied the impact of divertor poloidal magnetic flux expansion and flux tube flaring on detachment characteristics. In TCV, detachment characteristics were studied in the cusp/X-divertor configuration albeit with a long leg [64, 127, 128] with different target flux expansions $f_{\rm exp} = 2.8$–9.3. The experimental data and trends were also modeled using a two-dimensional edge transport code B2-EIRENE. Both the experiment and the modeling showed enhanced degrees of detachment with increased flux expansion. It was proposed that with increased flux expansion, a plasma plugging effect was responsible for better entrapment of neutrals. In NSTX detachment studies, a comparison of standard divertor configurations with lower and higher flux expansions also showed facilitated access to detachment with higher $f_{\rm exp}$ [129–131]. Recent SOLPS detachment simulations of the proposed HL-2M tokamak with carbon impurities and $P_{\rm SOL} \leqslant 12$ MW showed that the tripod divertor configuration (similar to the cusp/X-divertor) had a reduced heat flux and less sputtered impurities (compare to standard detached divertor) [132]. In DIII-D, recent cusp/X-divertor studies [133] demonstrated reduced particle and heat fluxes to the target, facilitated detachment onset, at ~20% lower upstream density and higher H-mode pedestal pressure than a standard divertor, in agreement with SOLPS modeling. However, the effect of the flaring geometry was not quantified. In recent TCV experiments [90], detachment characteristics were studied in a number of advanced magnetic divertor configurations in L-mode plasmas with ion ∇B drift direction away from the X-point, and 400–800 kW ohmic heating. Experiments with different divertor flux expansions $f_{\rm exp} = 2.0 - 8.5$ and a shorter divertor leg (compare to previous TCV experiments), and without flaring flux tubes, showed that increasing the flux expansion did not affect the detachment onset. A similar result (i.e., no effect on detachment onset) was obtained with flux tube flaring in the cusp/X-divertor configuration. Impurity (C III) emission region showed a reduced movement towards the x-point with a higher flux expansion, consistent with the hypothesis of detachment front stabilization by a flaring flux tube (albeit the hypothesis referred to

ionization-recombination front stabilization in the neutral-dominated region).

Long-legged divertors with and without additional X-points. A number of experiments and modeling efforts attempted to clarify the effect of the long poloidal leg on divertor plasma characteristics and detachment. In DIII-D high input power experiments (8–9 MW), consistent with expectations, lower divertor T_e and $q_{\rm peak}$ were found in configurations with longer legs (even with lower flux expansion) with and without radiative divertor that was induced using D_2 seeding and carbon radiation [126, 134, 135]. H-mode confinement, core Greenwald density and $Z_{\rm eff}$ were comparable with radiative divertor conditions for short and long leg configurations. In recent TCV detachment experiments with D_2 seeding (albeit in L-mode with ion ∇B drift direction away from the X-point), it was demonstrated that longer-leg configurations detached at lower n_e, interpreted as stronger reduction in ion flux to the target, higher densities could be achieved, and the detachment was 'deeper' [90]. The latter characteristic refers to a lower ion saturation current value measured by target Langmuir probes during detachment at the same n_e. Effects of a divertor leg length on divertor T_e, detachment characteristics and impurities were confirmed in modeling studies. One-dimensional modeling of MAST-U configurations was used to study parallel physics of a shorter and longer leg configurations [136]. Two-dimensional modeling of reactor concepts CFETR with carbon and D_2 seeding using SOLPS showed that longer leg configuration reached detachment at lower gas puffing rate (i.e., density) [137]. Modeling of SlimCS DEMO with a fusion power of 3 GW with argon seeding using the two-dimensional SONIC code demonstrated that a longer leg divertor with argon seeding was effective in increasing the impurity retention in the divertor, increasing divertor radiated power, and in obtaining full detachment, in comparison to a reference standard divertor case [9, 138, 139].

We discuss the status of the Super-X divertor next. An up-down symmetric Super-X divertor configuration is envisioned for the MAST Upgrade tokamak. A plasma-facing component geometry design that forms a up-down and toroidally symmetric divertor channel and an up-down symmetric set of eight divertor coil pairs are being implemented [91, 92]. In the meantime, several experiment and modeling studies attempted to clarify the integrated effect of the target major radius, divertor leg length and flux tube flaring on detachment. A DIII-D study [134, 135] conducted in lower power (1.2 MW) L-mode and higher power (4.5 MW) H-mode found that parallel heat flux $q_{\parallel}$ was strongly reduced with increasing $R_{\rm target}$, as was plasma temperature at the target, consistent with supporting SOLPS modeling results. In recent TCV density ramp experiments [90] conducted in L-mode with ion ∇B drift direction away from the X-point and in configurations at different strike point radii, a reduction in $q_{\parallel}$ was observed with higher radius. However, detachment density threshold and impurity emission front location were both found to be independent of strike point radius.

Two-dimensional transport modeling codes generally confirm the Super-X effects. A comprehensive assessment of the MAST-U Super-X divertor was performed using the two-dimensional code SOLPS [136, 140–145]. A variety of input powers were used $P_{\rm in} = 0.85$–1.7 MW in the modeling. Results without impurities included a significant reduction of plasma target temperatures and peak power loads at the outer targets compared to the standard divertor due to magnetic flux expansion and larger volumetric power loss in the divertor, and significantly better divertor closure with respect to neutrals [143, 145]. When classical $E \times B$ drifts and parallel currents were included in the model, up-down asymmetries of heat and temperatures were noted, which were not observed in the simulations without drifts [144], suggesting that detachment could be affected. When impurities (carbon) were included, the Super-X geometry reduced the density threshold for the transition to detachment by a significant factor (3–4) [142]. With extrinsic nitrogen seeding, Super-X divertors (with two (lower and higher) flux expansion values) detached at a lower impurity seeding rate than the standard divertor [141]. Simulations with 1.7 MW input power and intrinsic carbon predicted that under the same core plasma conditions, the Super X-divertor was strongly detached while the standard divertor was in a sheath-limited regime. The standard divertor needed a factor of 3 higher density or a factor of 4 less power (see Super-X) to detach [140]. Two-dimensional code SOLPS was used to model plasma transport in a compact fusion neutron source tokamak with 50 MW power exhausted in the Super-X divertor [146]. Even without impurities, a partially detached regime with 2–3 eV target temperatures was demonstrated, whereas the standard divertor remained in a sheath-limited regime with $T_e \sim 150$ eV. Same conclusions were reached in a similar computational assessment of another concept—a National High-Power Tokamak Experiment [147]. A study of the 500 MW input power Chinese DEMO reactor using the B2.5-EIRENE code concluded that adequate outer divertor heat loads (under 10 MW m^{-2}) and low divertor $T_e \leqslant 5$ eV could be obtained in the Super-X divertor configuration by raising density and without impurity seeding [10]. The inner divertor, however, had a potential for impurity sputtering because of high $T_e \leqslant 150$ eV. In another DEMO study using the SONIC codes, 500 MW of power was exhausted through a short-leg vertical target Super-X divertor with argon seeding [139, 148]. Efficient argon retention and less argon for the same radiated power fraction (~90% of input power) was found in a fully detached stable divertor solution, in comparison with the standard divertor detached solution.

The X-point target configuration was proposed as part of the high-field, high-performance advanced divertor and radio-frequency tokamak experiment (ADX) [57]. The X-point target configuration has been obtained in the TCV tokamak in L-mode with ion ∇B drift direction away from the X-point [90]. Density ramp discharges with D_2 seeding showed no indication of decreased detachment threshold, despite a 2 to 3-fold connection length increase, as compared to the standard divertor. The carbon radiation front appeared to stabilize in the vicinity of the secondary null near the divertor target. An assessment of the X-point target divertor configuration for power handling and detachment front control was carried out

using the two-dimensional code UEDGE for a 6–8 MW plasmas and 1% carbon similar to the ADX configuration [149]. A comparison of three long-legged configurations (the X-point target, Super-X and long-legged divertor) to the standard divertor showed significantly increased operation window of detachment and a stable fully detached divertor state. The X-point target was shown to maintain the low $T_e \sim 1$ eV fully detached state for twice the input power than other long legged configurations.

Radiative snowflake divertor. Divertor detachment with D_2 and neon seeding were studied in snowflake configurations in NSTX, DIII-D and TCV experiments [62].

In 4 MW NBI-heated H-mode plasmas in NSTX, the snowflake-minus configuration led to a partial detachment of primary connected strike points without additional D_2 seeding, otherwise inaccessible at the same upstream parameters in the standard divertor configuration [150–153]. H-mode confinement was unaffected. Higher radiation levels were produced in already detached snowflake-minus divertor configurations with additional D_2 or CD_4 seeding.

In DIII-D, radiative snowflake experiments were performed in two settings. Experiments performed in lower snowflake-minus or -plus configurations with D_2 seeding at $P_{SOL} = 3$–4 MW [153–155] showed that (compare to standard divertor) (1) both the radiative snowflake-minus and snowflake-plus were compatible with the H-mode albeit with confinement degradation with respect to the standard radiative divertor H-mode discharge with a similar core density; (2) a reduction of inter-ELM divertor heat fluxes was stronger in the snowflake configurations, leading to nearly complete power detachment; (3) carbon and deuterium emissions were more broadly distributed in the snowflake configurations, including the additional divertor legs, at divertor radiation fraction $f_{rad} \sim (0.5–0.7)P_{SOL}$ and otherwise similar edge and core parameters. Experiments were also performed using $P_{in} \sim 10$ MW with neon and D_2 seeding in a configuration that included an upper single null and a lower snowflake-minus (snowflake-DN) with ion ∇B drift away from the lower X-point. While the peak heat flux reduction was about 50% stronger in the radiative snowflake-DN than in the standard radiative DN divertor with comparable core confinement, neon accumulation was 30%–40% higher in the radiative snowflake-DN case.

Neon seeding was used in TCV ohmic plasmas (250–350 kW) to study radiated power distribution in the standard and snowflake-plus configurations. A modest increase in divertor radiation was observed in the snowflake. Studies with D_2 seeding demonstrated the opposite effect: total radiated power was systematically slightly higher in the standard divertor configuration. Recent TCV experiments in L-mode with ion ∇B drift direction away from the X-point [90] showed that in the snowflake-minus configuration, density onset of detachment (using density ramps) in the two outer strike points was similar to the standard divertor. Nitrogen seeding was used to study divertor radiated power distribution as a function of density in the snowflake-minus configuration.

Detachment in snowflake configurations was modeled for the existing and future experiments and concepts (general snowflake divertor modeling was reviewed in [62]). The two-dimensional multi-fluid codes presently in use do not have the capability to generate numerical grids for snowflake divertor configurations with multiple nulls. An exception is the three-dimensional code EMC3-EIRENE, however, it has a simplified trace impurity model and does not include recombination processes which are critical for detachment physics. Transport models used are also simplified and do not attempt to include fast convection in the high β_p region, a key theoretically predicted snowflake divertor property. Only recently these shortcomings started to be addressed [156, 157]. The UEDGE code has been extensively used to model snowflake configurations: snowflake-minus experiments in NSTX [152, 158, 159], NSTX Upgrade snowflake-minus divertor with neon and argon seeding and cryopumping [153, 160], the spherical tokamak based fusion nuclear science facility divertor with nitrogen seeding [160], and snowflake-plus configurations for a fusion development facility device [161, 162]. This modeling generally showed that increased plasma-wetted area and connection length, as well as increased radiated power loss fraction in the snowflake divertor led to divertor detachment either at a lower density, or at a lower impurity seeding fraction, as compared to the standard divertor. Modeling of TCV snowflake-minus configurations with 300–400 kW input power using EMC3-EIRENE code showed that parallel heat flux was reduced in the snowflake-minus, and, with impurity seeding, radiation was peaking between the nulls, at a distance from the main separatrix [163, 164]. The SOLPS code was used to model detachment in quasi-snowflake divertor configurations obtained in the EAST tokamak [165]. The modeling showed that the quasi-snowflake configuration could reach very low T_e and more reduced peak heat flux (see standard divertor) at a lower density. Indications of detachment were observed in the first EAST experiments [166]. Significant heat flux reduction was observed in SOLPS simulations of attached divertor regimes due to snowflake geometry effects in the planned HL-2M tokamak [167, 168] and the Chinese Fusion Experimental Tokamak Reactor [169]. Modeling of detachment in snowflake divertor configurations for these devices is also starting [132, 170]. The detached regime in the snowflake-minus configuration with nearly 12 MW of SOL power and carbon impurities in HL-2M was less sensitive on n_e^{sep} and also had reduced impurity density and Z_{eff}.

5. Discussion

The status of radiative divertor and detachment research in tokamak advanced magnetic divertor configurations has been reviewed. The renewed interest in advanced divertors in the last decade has driven recent experimental and modeling studies, however, many outstanding physics and engineering problems need to be addressed in order to qualify advanced divertor concepts as a tokamak reactor plasma–material interface. It is becoming clear that studies of advanced magnetic divertor configurations are to repeat essentially similar standard divertor studies to verify and validate the mechanisms that may facilitate detachment or enhance it.

Recent experiments and modeling have validated certain geometric features of the advanced configurations and their impact on detachment. The modeling is limited to two-dimensional fluid models that often include charge-state-resolved impurities. The ultimate questions, e.g., reduced detachment threshold in density, stabilization of detachment front, total radiation fraction, and seeded impurity screening, are often addressed by the modeling with a positive outcome, however, experiments show more complicated mechanisms.

High flux expansion divertor solutions appear to improve certain detachment characteristics. However, they face arguments w.r.t. engineering requirements for plasma facing component alignment as the field angles approach small values. Additional justification to these solutions is provided if the plasma is radiatively detached since the plasma-surface interaction region would receive a much reduced heat flux. The results reviewed above validate a number of long-legged divertor concepts, as expected. However, as in the past, long-legged divertor solutions face difficult, if not prohibitive, engineering and cost considerations. The upcoming MAST Upgrade experiment will provide critical data not only on the physics but also on engineering performance of the long-legged and Super-X divertor configurations. Based on the results reviewed above, some implicit physics effects, e.g., stabilization of the detachment front by flux tube flaring, will require more experiments and modeling validation. The radiative snowflake divertor concept also needs additional research to validate the predicted features, namely the convective plasma redistribution (the churning mode), its impact on detachment, and the scaling of sharing of heat fluxes over additional strike points.

Ultimately, the divertor solution must be as simple as possible, to be able to provide a reliable robust interface to mitigate high heat and erosion fluxes. For advanced divertor configurations with additional null points, such as the snowflake, cusp/X/tripod, Super-X, and X-point target, one of the critical questions is the placement of the additional null w.r.t. the SOL width λ_q. The placement is likely to affect detachment characteristics as it determines what fraction of the SOL power is exhausted in the divertor channel with enhanced features, such as the modified geometry and transport. These configurations also face additional challenges w.r.t. detachment stability and sensitivity to additional null control, as well as stability due to transient plasma events. A large safety margin in detachment parameters must be considered if these configurations are sensitive to time-varying effects.

One of the questions that was barely addressed in the experiments and modeling is the inner-outer divertor balance. If the divertor solution is up-down asymmetric, heat and particles tend to flow to the outer divertor strike point due to in-out area asymmetry and greater outer side transport. Most efforts have been focused on the outer divertor, neglecting the inner divertor, where some studies predicted high unmitigated heat fluxes and erosion. If harsh inner divertor conditions cannot be mitigated, up-down symmetric configurations may be more viable.

Much progress is expected in the advanced magnetic divertor configuration studies in the near-term. The existing experiments, such as TCV, DIII-D and EAST, will continue on-going studies, and new experiments, such as MAST-U, NSTX-U and HL-2M will come on-line in the next few years. New dedicated divertor research devices are also under consideration [57, 171, 172]. These experiments should enable developing an integrated divertor solution that may be based on one of the reviewed magnetic configurations, advanced target technologies, and compatibility with the core plasma requirements.

Acknowledgments

The author thanks Dr D D Ryutov (retired, formerly at Lawrence Livermore National Laboratory) and Dr D Meade (retired, formerly at Princeton Plasma Physics Laboratory) for insightful discussions. This work was performed under the auspices of the US Department of Energy by Lawrence Livermore National Laboratory under Contract DE-AC52-07NA27344.

References

[1] Furth H 1975 *Nucl. Fusion* **15** 487
[2] Pitcher C S and Stangeby P C 1997 *Plasma Phys. Control. Fusion* **39** 779
[3] Spitzer L 1958 *J. Phys. Fluids* **1** 253
[4] Feneberg W 1971 *Phys. Lett.* **36A** 125
[5] Feneberg W and Lackner K 1973 *Nucl. Fusion* **13** 549
[6] Oshiyama H 1975 *J. Phys. Soc. Japan Lett.* **39** 263
[7] ITER Physics Expert Group on Divertor, ITER Physics Expert Group on Divertor Modelling and Database and ITER Physics Basis Editors 1999 *Nucl. Fusion* **39** 2391
[8] Loarte A *et al* 2007 *Nucl. Fusion* **47** S203
[9] Asakura N *et al* 2013 *Nucl. Fusion* **53** 123013
[10] Zheng G-Y, Pan Y-D, Feng K-M, He H-D and Cui X-W 2013 *Chin. Phys. Lett.* **30** 015201
[11] Wischmeier M 2015 *J. Nucl. Mater.* **463** 22
[12] Loarte A 2001 *Plasma Phys. Control. Fusion* **43** 183
[13] Kawashima H *et al* 1999 *Nucl. Fusion* **39** 1679
[14] Kawashima H *et al* 2006 *Fusion Sci. Technol.* **49** 168
[15] Mazul I 2016 *Nucl. Fusion* **56** 126009
[16] Niedermeyer H *et al* 1980 *J. Nucl. Mater.* **93–94** 286
[17] Kesner J 1990 *Nucl. Fusion* **30** 548
[18] Owens D *et al* 1980 *J. Nucl. Mater.* **93–94** 213
[19] Matthews G 1995 *J. Nucl. Mater.* **220** 104
[20] Krasheninnikov S, Kukushkin A and Pshenov A 2016 *Phys. Plasmas* **23** 055602
[21] Barr W L 1991 *Fusion Technol.* **19** 498
[22] Jardin S *et al* 2006 *Fusion Eng. Des.* **80** 25
[23] Vlases G C 1993 *Plasma Phys. Control. Fusion* **35** B67
[24] Lipschultz B, Parra F and Hutchinson I 2016 *Nucl. Fusion* **56** 056007
[25] Ribe F L 1975 *Rev. Mod. Phys.* **47** 7
[26] Meade D M 1977 Divertors for impurity control and review of impurity effects in PPL tokamaks *Proc. Int. Symp. on Plasma Wall Interaction (Julich)* (Oxford: Pergamon) p 21
[27] Meade D 1914 private communication
[28] Shimomura Y and Maeda H 1978 *J. Nucl. Mater.* **76–77** 45
[29] Yoshikawa M, Tazima T, Shimomura Y, Kitsunezaki A and Maeda H 1975 *Proc. 5th Int. Conf. on Plasma Physics and Controlled Nuclear Fusion Research* vol I *(Tokyo, 1974)* (Vienna: IAEA) p 17

[30] Bortnikov A, Brevnov N and Gerasimov S 1977 *Proc. 8th Europ. Conf. on Controlled Fusion and Plasma Physics* vol I *(Prague)* p 41
[31] Bortniknov A *et al* 1979 *Proc. 7th Int. Conf. on Plasma Physics and Controlled Nuclear Fusion Research* vol 1 *(Innsbruck, 1978)* (Vienna: IAEA) p 387
[32] Keilhacker M *et al* 1981 Impurity control experiments in the ASDEX divertor tokamak *Plasma Physics and Controlled Nuclear Fusion Research 1980* vol II (*Nuclear Fusion Supplement*) (Vienna: IAEA) p 351
[33] Keilhacker M and Daybelge U 1981 *Nucl. Fusion* **21** 1497
[34] Becker W E G *et al* 1982 *J. Nuc. Mater.* **111–112** 337
[35] Keilhacker M and Lackner K 1982 *J. Nucl. Mater.* **111-112** 370
[36] Ohyabu N *et al* 1983 *Nucl. Fusion* **23** 295
[37] Seki S *et al* 1984 *J. Nucl. Mater.* **121** 422
[38] Lackner K and Keilhacker M 1984 *J. Nucl. Mater.* **128–129** 368
[39] Tenney F H and Lewin G 1974 A fusion power plant *PPPL Report* MATT-1050 R G Mills (ed)
[40] Mueller E, Behringer K and Niedermeyer H 1982 *Nucl. Fusion* **22** 1651
[41] Shimomura Y, Keilhacker M, Lackner K and Murmann H 1983 *Nucl. Fusion* **23** 869
[42] Shimada M *et al* 1982 *Nucl. Fusion* **22** 643
[43] Igitkhanov Y, Kukushkin A and Pistunovich V 1981 Heat and particle flow distribution and possibility of helium separation in the divertor channel of a tokamak reactor *Plasma Physics and Controlled Nuclear Fusion Research 1980* vol II (Vienna: IAEA) p 575
[44] Post D, Heifetz D and Petravic M 1982 *J. Nucl. Mater.* **111–112** 383
[45] Petravic M, Post D, Heifetz D and Schmidt J 1982 *Phys. Rev. Lett.* **48** 326
[46] Ioki K *et al* 1982 *Nucl. Eng. Des.* **73** 45
[47] Ohyabu N and Renner H 1998 *Contrib. Plasma Phys.* **1/2** 94
[48] Emmert G, Donhowe J and Mense A 1974 *J. Nucl. Mater.* **53** 39
[49] Conn R W, Kulcinski G L and Maynard C W 1976 *Nucl. Eng. Des.* **39** 5
[50] Tone T *et al* 1983 *Fusion Sci. Technol.* **4** 573
[51] Hill D *et al* 1995 *J. Nucl. Mater.* **220–222** 698
[52] Keeilhacker M and the ASDEX Team 1985 *Nucl. Fusion* **25** 1045
[53] Petrie T *et al* 2001 *J. Nucl. Mater.* **290–293** 935
[54] Petrie T *et al* 2008 *Nucl. Fusion* **48** 045010
[55] Petrie T *et al* 2006 *Nucl. Fusion* **46** 57
[56] Petrie T *et al* 2009 *Nucl. Fusion* **49** 065013
[57] Labombard B *et al* 2015 *Nucl. Fusion* **55** 053020
[58] Vijvers W *et al* 2013 Power exhaust in all geometric variations of the snowflake divertor on TCV *Meeting of The American Physical Society, Division of Plasma Physics* BAPS.2013.DPP.PP8.47
[59] Ryutov D 2007 *Phys. Plasmas* **14** 064502
[60] Ryutov D D and Umansky M V 2013 *Phys. Plasmas* **20** 092509
[61] Ryutov D and Umansky M 2010 *Phys. Plasmas* **17** 014501
[62] Ryutov D D and Soukhanovskii V A 2015 *Phys. Plasmas* **22** 110901
[63] Ryutov D, Cohen R, Rognlien T and Umansky M 2012 *Plasma Phys. Control. Fusion* **54** 124050
[64] Pitts R *et al* 2001 *J. Nucl. Mater.* **290–293** 940
[65] Synakowski E *et al* 2003 *Nucl. Fusion* **43** 1653
[66] Ryutov D D 2015 *J. Plasma Phys.* **81** 495810516
[67] Okada O 1998 *Fus. Technol.* **33** 130
[68] Ogawa Y, Yamamoto T, Yonezawa K and Ohyabu N 2000 *Fusion Eng. Des.* **48** 339
[69] Takase H 2001 *J. Phys. Soc. Japan* **70** 609
[70] Kotschenreuther M T, Valanju P M, Mahajan J W T R S and Pekker M 2004 Scrape off layer physics for burning plasmas and innovative divertor solutions *Proc. 20th Int. Conf. on Fusion Energy (Vilamoura, Portugal)* (Vienna: IAEA) Paper IC/P6-43
[71] Takizuka T, Tokunaga S, Hoshino K, Shimizu K and Asakura N 2015 *J. Nucl. Mater.* **463** 1229
[72] Haines M 1977 *Nucl. Fusion* **17** 811
[73] Kotschenreuther M, Valanju P, Covele B and Mahajan S 2013 *Phys. Plasmas* **20** 102507
[74] Covele B, Valanju P, Kotschenreuther M and Mahajan S 2014 *Nucl. Fusion* **54** 072006
[75] Ryutov D D, Cohen R H, Rognlien T D, Soukhanovskii V A and Umansky M V 2014 *Phys. Plasmas* **21** 054701
[76] Kotschenreuther M, Valanju P, Mahajan S and Wiley J 2007 *Phys. Plasmas* **14** 72502
[77] Tenney P and Lewin G 1972 Design considerations for divertors in toroidal fusion reactors *7th Symp. on Fusion Technology (Grenoble, France, 24–27 October)*
[78] Tenney F H 1974 *J. Nucl. Mater.* **53** 43
[79] Tenney F H 1976 A tokamak hybrid study *Joint US-USSR Symp. on Fusion-Fission Hybrid Reactors (Livermore, 13–16 July 1976)* (Princeton, NJ: Princeton University Press) Plasma Physics Laboratory Report PPPL-1284
[80] Conn R W, Kulcinski G L, Abdou M, Boom R W and Emmert G A 1974 Major design features of the conceptual D-T tokamak power reactor UWMAK-II *Report* UWFDM-114 U Wisconsin Fusion Technology Institute
[81] Conn R W and Kuo S C 1976 *Nucl. Eng. Des.* **45** 45
[82] Badger B, Kulcinski G L, Conn R W, Maynard C W and Audenaerde K 1975 UWMAK-II, A high performance, noncircular tokamak power reactor design *Report* UWFDM-150 U Wisconsin Fusion Technology Institute
[83] Yang T F and Conn R W 1976 *IEEE Trans. Plasma Sci.* **PS-4** 249
[84] Badger B, Kulcinski G L, Conn R W, Maynard C W and Audenaerde K 1977 TETR: A tokamak engineering test reactor to qualify materials and blanket components for early D-T fusion power reactors *Report* UWFDM-191 U Wisconsin Fusion Technology Institute
[85] Georgievsky A V *et al* 1975 Conceptual design of a divertor for a tokamak experimental power reactor *Proc. 6th Symp. on Engineering Problems of Fusion Research (San Diego, CA, USA)*
[86] Ohyabu N 1991 *JSPF* **11** 525
[87] Mcintosh S *et al* 2014 Engineering feasibility of the double decker divertor *25th IAEA Int. Conf. on Fusion Energy Conf. (St Petersburg, Russian Federation, 13–18 October 2014)* Paper FIP/P8-9
[88] Valanju P, Kotschenreuther M, Mahajan S and Canik J 2009 *Phys. Plasmas* **16** 056110
[89] Valanju P, Kotschenreuther M and Mahajan S 2010 *Fusion Eng. Des.* **85** 46
[90] Reimerdes H *et al* 2016 TCV experiments towards the development of a plasma exhaust solution *Proc. 26th IAEA FEC (Kyoto, Japan)* Paper EX/2-3
[91] Katramados I *et al* 2011 *Fusion Eng. Des.* **86** 1595
[92] Fishpool G *et al* 2013 *J. Nucl. Mater.* **438** S356
[93] Degrassie J, Deboo J, Mahdavi M, Ohyabu N and Shimada M J 1982 *Vac. Sci. Technol.* **20** 1222
[94] Mahdavi M 1986 *Trans. Am. Nucl. Soc.* **52** 159
[95] Mahdavi M A *et al* 1981 *Phys. Rev. Lett.* **47** 1602
[96] Mahdavi M *et al* 1982 *J. Nucl. Mater.* **111–112** 355
[97] Shimada M *et al* 1982 *J. Nucl. Mater.* **111–112** 362
[98] Groups D I 1980 *J. Nucl. Mater.* **93–94** 259 Part 1
[99] Ohyabu N 1981 *Nucl. Fusion* **21** 519
[100] Doublet III Groups 1980 *J. Nucl. Mater.* **93–94** 259
[101] Fonck R and Hulse R 1984 *Phys. Rev. Lett.* **52** 530

[102] Shimada M *et al* 1981 *Phys. Rev. Lett.* **47** 796
[103] Boo J D *et al* 1982 *Nucl. Fusion* **22** 572
[104] Maeno M *et al* 1981 *Nucl. Fusion* **21** 1474
[105] Kaye S *et al* 1984 *J. Nucl. Mater.* **121** 115
[106] Ohyabu N *et al* 1985 *Nucl. Fusion* **25** 49
[107] Wagner F *et al* 1982 *Phys. Rev. Lett.* **49** 1408
[108] Meade D *et al* 1981 *Nucl. Fusion Suppl.* **1** 665
[109] Haas G, Keilhacker M, Poschenrieder W, Vernickel H and Wagner F 1976 *J. Nucl. Mater.* **63** 92
[110] Bell M *et al* 1984 *J. Nucl. Mater.* **121** 132
[111] Fonck R *et al* 1982 *J. Nucl. Mater.* **111–112** 343
[112] Nagami M *et al* 1980 *Nucl. Fusion* **20** 1325
[113] Nagami M *et al* 1981 *Nucl. Fusion Suppl.* **2** 367
[114] Miya N *et al* 1984 *J. Nucl. Mater.* **121** 126
[115] Shimada M *et al* 1984 *J. Nucl. Mater.* **128–129** 340
[116] Kahn C *et al* 1984 *J. Nucl. Mater.* **128–129** 172
[117] Kahn C *et al* 1986 *Nucl. Fusion* **26** 73
[118] Shimada M and The JAERI TEAM 1984 *J. Nucl. Mater.* **121** 184
[119] Ueda N, Kasai M, Tanaka M, Sugihara M and Sengoku S 1988 *Nucl. Fusion* **28** 1183
[120] Ueda N, Itoh K and Itoh S-I 1989 *Nucl. Fusion* **29** 173
[121] Kukushkin A *et al* 2003 *Fus. Eng. Des.* **65** 355
[122] Kukushkin A, Pacher H, Kotov V, Pacher G and Reiter D 2011 *Fus. Eng. Des.* **86** 2865
[123] Kukushkin A, Pacher H and Pitts R J 2015 *Nuc. Mater* **463** 586
[124] Loarte A *et al* 1999 *J. Nucl. Mater.* **266–269** 587
[125] Loarte A and Harbour P 1992 *Nucl. Fusion* **32** 681
[126] Petrie T *et al* 2015 *J. Nucl. Mater.* **463** 1225
[127] Pitts R *et al* 1997 *J. Nucl. Mater.* **241–243** 867
[128] Pitts R *et al* 1999 *J. Nucl. Mater.* **266** 648
[129] Soukhanovskii V A *et al* 2005 *J. Nucl. Mater.* **337–339** 475
[130] Soukhanovskii V A *et al* 2009 *Phys. Plasmas* **16** 022501
[131] Soukhanovskii V A *et al* 2009 High flux expansion divertor studies in NSTX *36th EPS Conf. on Plasma Phys. (Sofia, Bulgaria)* arXiv:0912.4281
[132] Zheng G Y *et al* 2016 *Nucl. Fusion* **56** 126013
[133] Covele B *et al* 2016 X-divertors for deeper detachment without degrading the DIII-D H-Mode *Proc. 26th IAEA FEC (Kyoto, Japan)* Paper EX/P3-28
[134] Petrie T *et al* 2013 *J. Nucl. Mater.* **438** S166
[135] Petrie T *et al* 2013 *Nucl. Fusion* **53** 113024
[136] Havlickova E *et al* 2013 *Plasma Phys. Control. Fusion* **55** 065004
[137] Zhang C *et al* 2016 *Fus. Eng. Des.* **109–111** 1119 Part B
[138] Hoshino K *et al* 2012 *Contrib. Plasma Phys.* **52** 550
[139] Asakura N *et al* 2013 *Fusion Sci. Technol.* **63** 70
[140] Havlickova E *et al* 2015 *Plasma Phys. Control. Fusion* **57** 115001
[141] Havlickova E, Wischmeier M, Lipschultz B and Fishpool G 2015 *J. Nucl. Mater.* **463** 1209
[142] Havlickova E, Wischmeier M and Fishpool G 2014 *Contrib. Plasma Phys* **54** 448
[143] Havlickova E, Fundamenski W, Wischmeier M, Fishpool G and Morris A 2014 *Plasma Phys. Control. Fusion* **56** 075008
[144] Rozhansky V *et al* 2013 *Plasma Phys. Control. Fusion* **55** 035005
[145] Havlickova E, Fundamenski W, Wischmeier M, Fishpool G and Coster D 2013 *J. Nucl. Mater.* **438** S545–9
[146] Kotschenreuther M *et al* 2010 *Nucl. Fusion* **50** 035003
[147] Canik J *et al* 2009 *J. Nucl. Mater.* **390–391** 315
[148] Asakura N *et al* 2015 *J. Nucl. Mater.* **463** 1238
[149] Umansky M *et al* 2016 Assessment of X-point target divertor configuration for power handling and detachment front control *Proc. 26th IAEA FEC (Kyoto, Japan)* Paper TH/P6-32
[150] Soukhanovskii V *et al* 2011 *Nucl. Fusion* **51** 012001
[151] Soukhanovskii V *et al* 2011 *J. Nucl. Mater.* **415** S365
[152] Soukhanovskii V *et al* 2012 *Phys. Plasmas* **19** 082504
[153] Soukhanovskii V A *et al* 2016 *IEEE Trans. Plasma Sci.* **44** 3445
[154] Soukhanovskii V A *et al* 2014 Developing physics basis for the radiative snowflake divertor at DIII-D *Proc. 25th IAEA FEC–IAEA CN-221 (St. Petersburg, 16–21 October 2014)* Paper EX/7-4
[155] Soukhanovskii V *et al* 2015 *J. Nucl. Mater.* **463** 1191
[156] Rognlien T D 2014 *Meeting of the American Physical Society, Division of Plasma Physics* BAPS.2014.DPP.GI1.4
[157] Izacard O and Umansky M V 2017 *Comp. Phys. Comm.* (submitted)
[158] Meier E *et al* 2015 *J. Nucl. Mater.* **463** 1200
[159] Meier E, Soukhanovskii V, Gerhardt S, Menard J and Rognlien T 2014 *Contrib. Plasma Phys.* **54** 454
[160] Meier E, Gerhardt S, Menard J, Rognlien T and Soukhanovskii V 2015 *Nucl. Fusion* **55** 086002
[161] Umansky M V, Bulmer R H, Cohen R H, Rognlien T D and Ryutov D D 2009 *Nucl. Fusion* **49** 075005
[162] Umansky M, Rognlien T, Ryutov D and Snyder P 2010 *Contrib. Plasma Phys.* **50** 350
[163] Lunt T *et al* 2014 *Plasma Phys. Control. Fusion* **56** 035009
[164] Lunt T *et al* 2016 *Plasma Phys. Control. Fusion* **58** 045027
[165] Si H *et al* 2016 *Phys. Plasmas* **23** 032502
[166] Calabro G *et al* 2015 *Nucl. Fusion* **55** 083005
[167] Zheng G-Y, Pan Y-D, Feng K-M, He H-D and Cui X-W 2012 *Chin. Phys. Lett.* **29** 105202
[168] Zheng G *et al* 2016 *Fus. Eng. Design* **112** 450
[169] Mao S *et al* 2015 *J. Nucl. Mater.* **463** 1233
[170] Wu H *et al* 2015 *He Jishu/Nucl. Tech.* **38** 110601
[171] Albanese R and on behalf of the WPDTT2 Team, and the DTT Project Proposal Contributors 2017 *Nucl. Fusion* **57** 016010
[172] Wan B *et al* 2014 *IEEE Trans. Plasma Sci.* **42** 495